ChemComm

Solvation-Dependent Switching of Solid-state Luminescence of a Fluorinated Aromatic Tetrapyrazole

Journal:	*ChemComm*
Manuscript ID	CC-COM-05-2019-003932.R1
Article Type:	Communication

COMMUNICATION

Solvation-Dependent Switching of Solid-state Luminescence of a Fluorinated Aromatic Tetrapyrazole

Received 00th January 20xx,
Accepted 00th January 20xx

DOI: 10.1039/x0xx00000x

Zhenglin Zhang, Thien Lieu, Chia-Hua Wu, Xiqu Wang, Judy I. Wu, Olafs Daugulis and Ognjen Š. Miljanić*

Creating stimuli-responsive materials with switchable solid-state luminescence remains a challenge. We report that the solvation of a noval organic fluorophore can be ulitized to prepare such a material, which emits in the blue (442–446 nm) region when wet and green (497–503 nm) when dry.

Solid-state materials that respond to external stimuli with switchable luminescence have been attracting attention due to their applications in the construction of physical and chemical sensors, displays, and recording devices.[1] Organic and organometallic molecules with different solid-state packing modes have been widely used to construct such materials. Switching of the luminescence is usually induced by stimuli such as light, mechanical grinding, temperature, shearing, pressure, and solvents, which can change materials' intramolecular conformation[2] and intermolecular arrangement, resulting in the formation of excimers[3a–f] or exciplexes,[3g] amorphization,[4a–d] and/or phase transitions.[4e–i]

Solvent-based switching of solid-state luminescence shows advantages in recording, as the liquid state of solvents allows easy control of the stimuli position—analogous to writing ink,[3f,g] and can be utilized to detect volatile organic compounds (VOCs).[5,6] There are different ways for solvents to change luminescence. In organometallic materials, solvent molecules can change luminescence by (*a*) directly coordinating to a metal cation,[6a–d] (*b*) changing their position or occupancy number in the void space of crystals,[6e–i] or (*c*) simple fuming without the net uptake of solvent molecules.[6j] However, traditional organic fluorophores often suffer from aggregation-caused quenching problems, limiting their use in the development of organic solid-state luminescent emitters.[7] The emerging classes of organic compounds showing aggregation-induced emission (AIE) are overcoming such limitations.[7] For organic materials with solid-state luminescence, the emission color switching by fuming an amorphous material was reported,[8] but the use of crystal solvation as a strategy to switch the solid-state emission in organics was only recently reported by Yin.[9] Considering the importance of solvents in the behavior of stimuli-responsive materials, more details on their role in the building of the basic units with organic fluorophores are acutely needed. Here, we report two crystals of a new organic fluorophore **1** with different solvation modes of DMF solvent. One of them shows solid-state fluorescence which switches from blue to green upon drying (and vice versa), while the other has a constant cyan fluorescence. This difference is explained by the different roles of DMF molecules in the intermolecular packing.

Recently, our group synthesized a number of porous molecular crystals (PMCs) with rigid aromatic "arms" built from fluoroarenes and pyrazoles, which promote intermolecular hydrogen bonds and [π···π] stacking that hold the porous structures in place.[10] Such PMCs and their precursors show fast adsorption of fluorinated compounds,[11a] adsorbate-induced piezochromism,[11b] and aggregation and self-assembly induced emission.[11c,d] Our previous work has explored linear, bent, and trigonal geometries of precursors to PMCs. In this work, we set

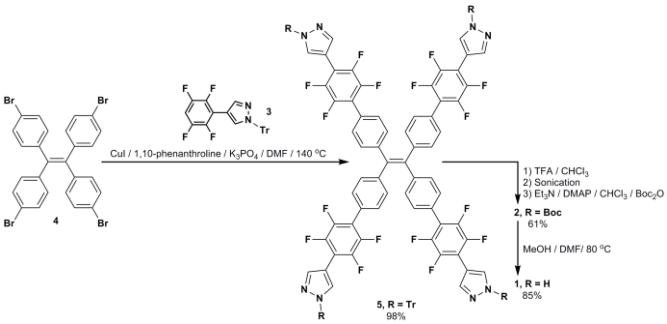

Scheme 1. The synthesis of compound **1**.

Department of Chemistry, University of Houston,
112 Fleming Building, Houston, TX 77204-5003, USA.
E-mail: miljanic@uh.edu; Tel: + 1 832 842-8827.
Electronic Supplementary Information (ESI) available: [details of any supplementary information available should be included here]. See DOI: 10.1039/x0xx00000x

out to examine the properties of a tetragonal geometry wherein four arms are linked to the central ethylene core. As shown in Scheme 1, we designed the organic fluorophore **1** by grafting the arm of fluorinated benzene and pyrazole to tetraphenylethylene, which is a classic compound exhibiting AIE effect and often used in stimuli-responsive materials.[7] The synthetic procedures and characterization data for the new compounds can be found in the ESI.

Absorption and emission spectra of **1** and **2** in the THF (good solvent)/H_2O (poor solvent) mixed solvent system were collected, which show that both compounds are AIE active (Figure 1, and Tables S1 and S2). Both **1** and **2** show very similar absorption and emission spectra when water fraction f_w = 0%, as they share the same conjugation system. The relative emission intensity (I/I_0) of **1** increased to 27.3–29.6 with visible green fluorescence under UV light (365 nm) when the H_2O volume fraction (f_w) exceeded 75% (Figure 1c). The I/I_0 of **2** also enhanced to 13.7–18.8 with $f_w \geq 45\%$, but the visible emission color changed significantly from blue (f_w = 45–75%) to cyan (f_w = 90%) and then to green (f_w = 98%) (Figure 1f). In the absorption spectra of **1** in mixed solvent at $f_w \geq 75\%$, a new peak around 393 nm appeared, which may be from a dimer formed by tight intermolecular interactions between electron-rich pyrazole donor and electron-poor tetrafluorobenzene acceptor as aggregation.[12] However, the absorption peaks of **2** just changed in a narrow region (279–309 nm) in the mixed solvent system, and no such peak around 393 nm was observed even when f_w reached 98%. Tentatively, we explain this observation by the bulky *tert*-butyloxycarbonyl groups of **2** hindering the tighter intermolecular approach and interaction between molecules of **2**. The different emission behaviors of **1** and **2** in H_2O/THF suggest that it is possible to achieve different solid-state luminescence based on the same π conjugation system. We next set out to test whether a single compound could be coerced into such different emission behaviors through variations in crystal packing.

Compound **1** crystallizes in two distinct forms. Crystals **1A** were produced by the slow evaporation of the solution obtained after a solvothermal reaction (80 °C, 24 h) of compound **2** (2.1 mg/mL) in a mixed solvent of DMF/MeOH. The crystals of **1A** are long, straight, and rod-like in their mother liquor. They are colorless under white light and show an emission peak (λ_{em}) at 446 nm with visible blue color under UV irradiation (Figure 2a and c, labelled as "wet 1"). Surprisingly, when crystals of **1A** were filtered and air-dried, they became yellow. Such sensitive color change prompted us to explore **1A**'s emission under dry conditions too. To do so, the mother liquor of the wet **1A** was first adsorbed by a Kimwipe and then the crystals were dried in vacuo at room temperature for 10 min. After the first drying, the crystals remained long, straight, and rod-shaped but became opaque and small cracks appeared on their surface. They showed λ_{em} at 503 nm with visible green fluorescence under UV irradiation (Figure 2a and c, "dry 2"). Re-wetting the sample by 1–2 drops of DMF recovered its original emission spectrum with blue emission color (Figure 2a, "wet 3"). The alternation of wet and dry conditions resulted in the reversible switching of emission color from blue to green over

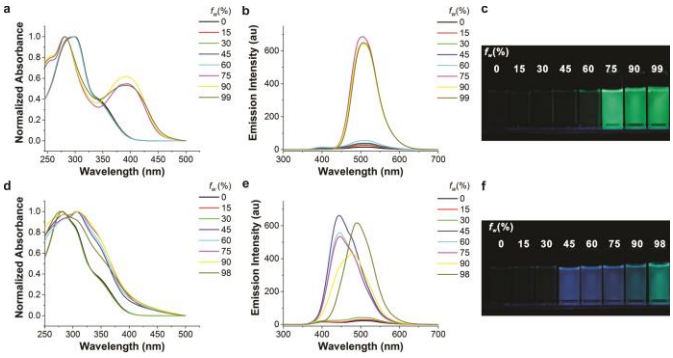

Figure 1. The absorption (**a** and **d**) and emission (**b**, λ_{exc} = 298 nm and **e**, λ_{exc} = 282 nm) spectra, and digital photos under UV irradiation (**c** and **f**, λ_{exc} = 365 nm) of **1** (**a**-**c**, 10 μM) and **2** (**d**-**f**, 10 μM) in THF/H_2O solvent system with varying f_w.

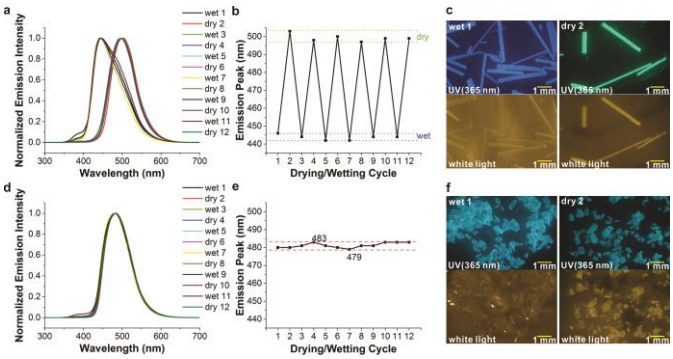

Figure 2. Behavior of crystal **1A** (**a**-**c**) and **1B** (**d**-**f**) during wetting and drying cycles: emission spectra (**a** and **d**, λ_{exc} = 298 nm) and the emission peak (**b** and **e**) of crystals as a function of wetting and drying. Digital microscope photos (**c** and **f**) of wet as-prepared (left) and then dried (right) crystals under UV (365 nm) and white light; Note: "wet 1" of crystal **1A** contained DMF and a small (<15%) amount of MeOH leftover from the synthesis. Other "wet" crystals have been wetted with DMF only.

six wetting-drying cycles (Figure 2a-b and Figure S10, and a video in ESI).

On the other hand, recrystallization of the hot DMF solution of compound **1** (10 mg/mL) generated crystals of **1B**, which are yellow and block-like, showing λ_{em} at 480 nm with visible cyan emission under UV light (Figure 2d and f, "wet 1"). Subjected to the same drying and wetting cycles as **1A**, the crystals of **1B** changed the λ_{em} only within a very narrow range (479–483 nm) and kept their cyan fluorescence over six wetting-drying cycles (Figure 2d-f and Figure S11). The excitation spectra were also tested for crystals **1A** and **1B** (see Figure S12), which show that a new peak around 430 nm appeared after crystals **1A** were dried. However, the excitation spectra of **1B** almost overlapped at the long wavelength side. All these emission and excitation spectra under the wet and dry conditions indicate that **1A** is stimuli-responsive to DMF solvent, but **1B** is not. To explain the

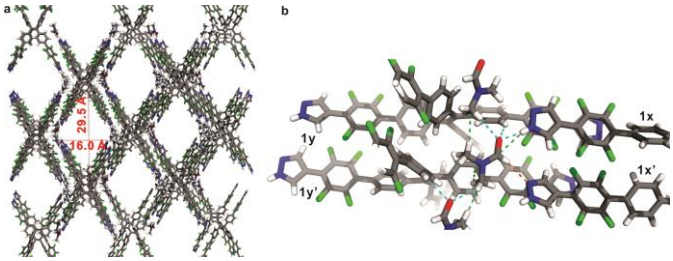

Figure 3. The structure of single crystal **1A**: (**a**) the framework formed by **1** and DMF; (**b**) the intermolecular interactions established by a DMF molecule. Note: the cyan, orange, and green dash lines represent O···H, N···H, and C···H interactions, respectively. Element colors: H—white, N—blue, C—gray, F—green, O—red.

observed difference, single X-ray diffraction (XRD) analyses were carried out on both crystals.

Crystals of **1A** show a monoclinic space group *C*2/c with half a molecule of **1** and one DMF molecule in the asymmetric unit. Molecules of **1** and DMF form a framework with parallelogram-shaped void channels (16.0 × 29.5 Å, Figure 3a) along the crystallographic *c* axis. These channels are filled with disordered solvent molecules (DMF and MeOH) under wet conditions.[13] Each DMF molecule shows strong interactions with four molecules of **1** and two other molecules of DMF (Figure 3b). The oxygen atom of the central DMF forms hydrogen bonds with **1x** and **1y**. The formyl group of the DMF as hydrogen bond donor interacts with a pyrazole group of **1x'**. There is also a C–H···C(π) interaction between a methyl group of DMF and a benzene ring of **1y'**. Along the crystallographic *c* axis, each DMF molecule also interacts with two adjacent DMF molecules by O···H–C hydrogen bonds. The DMF molecules therefore form an infinite hydrogen-bonded chain along the *c* axis, while also hydrogen bonding with neighboring molecules of **1**, forming the void channels structure. More details of the structure of crystal **1A** can be found in Figure S13-15. The important role of DMF in forming such a framework also means that the crystal structure is unstable after drying. Although the single crystal structure of the dried **1A** was not obtained due to the poor quality of dried crystals, the powder XRD data supports that the packing mode changed during wetting and drying cycles (see Figure S16).

To further understand the importance of DMF in maintaining the framework of **1A**, a theoretical simulation was carried out to show the stability of a dimer (Figure 4).[10b] The initial dimer model is based on the dimer extracted from the single crystal structure of **1A**, where the arms (two from C_1 atom and two from C_4 atom) not involved in the intermolecular interactions in the dimer are replaced with hydrogens to save the computational expense. The dihedral angle of C_1–C_2–C_3–C_4, and the angles of C_1–C_2–C_3 and C_2–C_3–C_4 are fixed, which ensure that the orientation of the two C=C bonds are always kept as in the original crystal structure. The calculation scanned the energy of each optimized dimer structure along the distance of C_2-C_3 with an interval of 0.2 Å, which changes the relative position of the two adjacent arms. As shown in Figure 4b and c, a more stable dimer with 9.9 kcal mol^{-1} lower energy can be found as the distance of C_2-C_3 decreases from 20.2 Å of the initial dimer to 15.6 Å. Such stable structure shows a larger overlapped area of the intermolecular aromatic rings with a shorter interlayer distance, which may be the reason why the emission color of crystal **1A** shifts from blue to green upon drying.

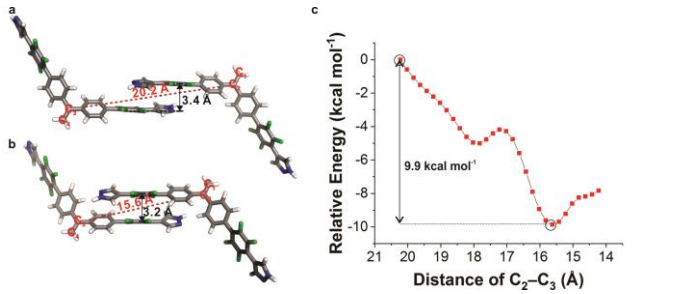

Figure 4. (**a**) The initial dimer model. (**b**) The optimized dimer with the lowest structure energy. (**c**) The relation between the C_2–C_3 distance and the relative energy of the dimer. The calculations were performed at the B3LYP-D3/6-31G(d) level by using Gaussian 16.[17]

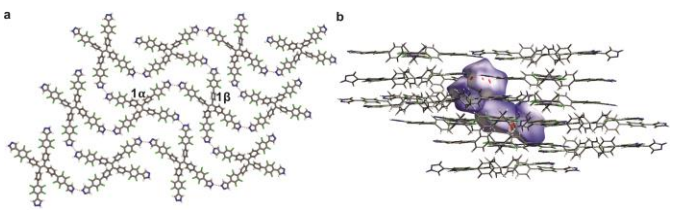

Figure 5. (**a**) The intermolecular interactions among molecules of **1** in a single layer and (**b**) the structure established by four spatially close DMF molecules, covered by Hirshfeld surfaces, with neighbouring molecules of **1** in crystal **1B**. The orange dash line represents N···H interaction.

Crystal **1B** crystallizes in a triclinic space group $P\bar{1}$ with two molecules of **1** and four molecules of DMF in the asymmetric unit.[13] There are two conformations in crystal **1B**, indicated as **1α** and **1β**, where the pyrazole groups are almost coplanar with the central double bond. However, crystal **1A** just has one conformation **1γ**, whose pyrazole groups are nearly perpendicular to the central double bond (see Figure S17 and Table S5). Such difference results in different packing modes of crystals. Each **1α** (or **1β**) connects with four molecules of **1β** (or **1α**) by N···H–N hydrogen bonds as donors or acceptors in a layer (Figure 5a). Each layer combines with adjacent layers by a series of intermolecular interactions and short contacts (see Figure S18), which results in a much tighter packing mode of crystal **1B** than that of crystal **1A**, as supported by the analyses of void space, which are 527.02 Å^3 (7.8% of unit cell volume) in crystal **1B** and 2522.2 Å^3 (29.4% of unit cell volume) in crystal **1A** (for details, see Figure S19). In crystal **1B**, each four spatially close DMF molecules are closely trapped in a void formed by molecules of **1**, which can be observed easily by Hirshfeld surfaces covering four such DMF molecules (Figure 5b, and Figure S20 and 21).[14] After dried in vacuo overnight, crystals of **1B** kept similar unit cell parameters (triclinic, a = 17.08(10) Å, b = 21.15(12) Å, c = 21.57(13) Å, α = 94.5(2) °, β = 111.37(17) °, γ = 110.82(13) °) as those of the single crystal **1B** under wet conditions (Table S4).

The calculated energy gaps between the optimized first excited state and ground state of the three types of molecule **1**, surrounding by neighbouring molecules generated by Hirshfeld surface analysis, are 2.52 eV (492 nm), 2.51 eV (494 nm), and 2.74 eV (452 nm) for **1α** and **1β** of **1B**, and **1γ** of **1A**, respectively. These values agree with experimentally obtained λ_{em} values of 479–483 nm (**1B**) and 442–446 nm (**1A**, wet). Details of these calculations are provided in Figure S22.

In summary, our analyses above show that the tight packing mode of crystal **1B** neatly traps the DMF molecules, making their escape and reentry impossible during the drying and wetting cycles; therefore, its emission remains constant. On the other hand, the framework of crystal **1A** established with DMF and **1** is loosely packed, and can easily shift from one occupancy mode to another with drying and re-wetting and that change is reported on with vivid switching of the emission color of **1A**. Our results suggest that the solvation of crystals could be used in the design of stimuli-responsive materials: different solvation of one and the same fluorophore can be an efficient way to

construct stimuli-responsive materials by using solvent molecules to adjust fluorophores' packing mode.

We acknowledge the financial support from the National Science Foundation (awards DMR-1507664 to O. Š. M. and O. D., and CHE-1751370 to J. I. W.) and the Welch Foundation (awards E-1768 to O. Š. M. and E-0044 to O. D.). Computational resources were provided by the uHPC cluster, managed by the University of Houston and acquired through support from the National Science Foundation (MRI-1531814).

Notes and references

1 (*a*) Y. Sagara, S. Yamane, M. Mitani, C. Weder and T. Kato, *Adv. Mater.*, 2016, **28**, 1073; (*b*) Z. Qiu, W. Zhao, M. Cao, Y. Wang, J. W. Y. Lam, Z. Zhang, X. Chen and B. Z. Tang, *Adv. Mater.*, 2018, **30**, 1803924; (*c*) L. Bai, P. Bose, Q. Gao, Y. Li, R. Ganguly and Y. Zhao, *J. Am. Chem. Soc.*, 2017, **139**, 436; (*d*) Y. Ren, S. Xie, E. S. Grap, A. K. Inge and O. Ramström, *J. Am. Chem. Soc.*, 2018, **140**, 13640.

2 (*a*) B. Shao, M. Baroncini, H. Qian, L. Bussotti, M. D. Donato, A. Credi and I. Aprahamiam, *J. Am. Chem. Soc.*, 2018, **140**, 12323; (*b*) Z. Wang, Z. Ma, Y. Wang, Z. Xu, Y. Luo, Y. Wei and X. Jia, *Adv. Mater.*, 2015, **27**, 6469; (*c*) Z. Ma, Z. Wang, X. Meng, Z. Ma, Z. Xu, Y. Ma and X. Jia, *Angew. Chem. Int. Ed.*, 2016, **55**, 519; (*d*) Z. Ma, M. Teng, Z. Wang, S. Yang and X. Jia, *Angew. Chem. Int. Ed.*, 2013, **52**, 12268.

3 (*a*) M. Teng, X. Jia, S. Yang, X. Chen and Y. Wei, *Adv. Mater.*, 2012, **24**, 1255; (*b*) L. Liu, X. Wang, N. Wang, T. Peng and S. Wang, *Angew. Chem. Int. Ed.*, 2017, **56**, 9160; (*c*) Y. Sagara and T. Kato, *Angew. Chem. Int. Ed.*, 2011, **50**, 9128; (*d*) Y. Sagara and T. Kato, *Angew. Chem. Int. Ed.*, 2008, **47**, 5175; (*e*) K. Nagura, S. Saito, H. Yusa, H. Yamawaki, H. Fujihisa, H. Sato, Y. Shimoikeda and S. Yamaguchi, *J. Am. Chem. Soc.*, 2013, **135**, 10322; (*f*) S. Yoon, J. W. Chung, J. Gierschner, K. S. Kim, M. Choi, D. Kim and S. Y. Park, *J. Am. Chem. Soc.*, 2010, **132**, 13675; (*g*) S. K. Park, I. Cho, J. Gierschner, J. H. Kim, J. H. Kim, J. E. Kwon, O. K. Kwon, D. R. Whang, J. Park, B. An and S. Y. Park, *Angew. Chem. Int. Ed.*, 2016, **55**, 203.

4 (*a*) X. Luo, J. Li, C. Li, L. Heng, Y. Q. Dong, Z. Liu, Z. Bo and B. Z. Tang, *Adv. Mater.*, 2011, **23**, 3261; (*b*) W. Z. Yuan, Y. Tan, Y. Gong, P. Lu, J. W. Y. Lam, X. Y. Shen, C. Feng, H. H. Sung, Y. Lu, I. D. Williams, J. Z. Sun, Y. Zhang and B. Z. Tang, *Adv. Mater.*, 2013, **25**, 2837; (*c*) H. Ito, T. Saito, N. Oshima, N. Kitamura, S. Ishizaka, Y. Hinatsu, M. Wakeshima, M. Kato, K. Tsuge and M. Sawamura, *J. Am. Chem. Soc.*, 2008, **130**, 10044; (*d*) Y. Sagara, T. Mutai. I. Yoshikawa and K. Araki, *J. Am. Chem. Soc.*, 2007, **129**, 1520; (*e*) M. Jin, T. Seki and H. Ito, *J. Am. Chem. Soc.*, 2017, **139**, 7452; (*f*) Y. Dong, B. Xu, J. Zhang, X. Tan, L. Wang, J. Chen, H. Lv, S. Wen, B. Li, L. Ye, B. Zou and W. Tian, *Angew. Chem. Int. Ed.*, 2012, **51**, 10782; (*g*) Y. Liu, Q. Zeng, B. Zou, Y. Liu, B. Xu and W. Tian, *Angew. Chem. Int. Ed.*, 2018, **57**, 15670; (*h*) A. L. Balch, *Angew. Chem. Int. Ed.* 2009, **48**, 2641; (*i*) B. Y. Zhao, H. Gao, Y. Fan, T. Zhou, Z. Su, Y. Liu and Y. Wang, *Adv. Mater.*, 2009, **21**, 3165.

5 S. Nakajima, K. Albrecht, S. Kushida, E. Nishibori, T. Kitao, T. Uemura., K. Yamamoto, U. H. F. Bunz and Y. Yamamoto, *Chem. Commun*., 2018, **54**, 2534.

6 (*a*) K. R. England, S. H. Lim, L. M. C. Luong, M. M. Olmstead and A. L. Balch, *Chem. Eur. J.*, 2019, **25**, 874; (*b*) A. Laguna, T. Lasanta, J. M. López-de-Luzuriaga, M. Monge, P. Naumov and M. E. Olmos, *J. Am. Chem. Soc.*, 2010, **132**, 456; (*c*) T. Lasanta, M. E. Olmos, A. Laguna, J. M. López de Luzuriaga and P. Naumov, *J. Am. Chem. Soc.*, 2011, **133**, 16358; (*d*) C. E. Strasser and V. J. Catalano, *J. Am. Chem. Soc.*, 2010, **132**, 10009; (*e*) S. H. Lim, M. M. Olmstead and A. L. Balch, *Chem. Sci*, 2013, **4**, 311; (*f*) S. H. Lim, M. M. Olmstead and A. L. Balch, *J. Am. Chem. Soc.*, 2011, **133**, 10229; (*g*) M. A. Mansour, W. B. Connick, R. J. Lachicotte, H. J. Gysling and R. Eisenberg, *J. Am. Chem. Soc.*, 1998, **120**, 1329; (*h*) T. J. Wadas, Q. Wang, Y. Kim, C. Flaschenreim, T. N. Blanton and R. Eisenberg, *J. Am. Chem. Soc.*, 2004, **126**, 16841; (*i*) M. Jin, T. Sumitani, H. Sato, T. Seki and H. Ito, *J. Am. Chem. Soc.*, 2018, **140**, 2875; (*j*) M. A. Malwitz, S. H. Lim, R. L. White-Morris, D. M. Pham, M. M. Olmstead and A. L. Balch, *J. Am. Chem. Soc.*, 2012, **134**, 10885.

7 (*a*) H. Feng, Y. Yuan, J. Xiong, Y. Zheng and B. Z. Tang, *Chem. Soc. Rev.*, 2018, **47**, 7452; (*b*) M. Gao and B. Z. Tang, *ACS Sens.*, 2017, **2**, 1382; (*c*) J. Mei, N. L. C. Leung, R. T. K. Kwok, J. W. Y. Lam and B. Z. Tang, *Chem. Rev.*, 2015, **115**, 11718; (*d*) J. Mei, Y. Hong, J. W. Y. Lam, A. Qin, Y. Tang and B. Z. Tang, *Adv. Mater.*, 2014, **26**, 5429; (*e*) Y. Hong, J. W. Y. Lam and B. Z. Tang, *Chem. Soc. Rev.*, 2011, **40**, 5361; (*f*) Y. Hong, J. W. Y. Lam, and B. Z. Tang, *Chem. Commun.*, 2009, 4332.

8 (*a*) J. Wang, J. Mei, R. Hu, J. Z. Sun, A. Qin and B. Z. Tang, *J. Am. Chem. Soc.*, 2012, **134**, 9956; (*b*) S. A. Sharber, K. Shih, A. Mann, F. Frausto, T. E. Haas, M. Nieh and S. W. Thomas, *Chem. Sci.*, 2018, **9**, 5415; (*c*) Y. Matsunaga and J. Yang, *Angew. Chem. Int. Ed.*, 2015, **54**, 7985. The recovering effect of solvent on solid-state emission of organic fluorophores can also be found in 2d, 3a,f, g, and 4b.

9 Z. Wu, S. Mo, L. Tan, B. Fang, Z. Su, Y. Zhang and M. Yin, *Small*, 2018, **14**, 1802524.

10 (*a*) T.-H. Chen, I. Popov, W. Kaveevivitchai, Y.-S. Chuang, Y. Chen, O. Daugulis, A. J. Jacobson and O. Š. Miljanić, *Nat. Commun.*, 2014, **5**, DOI: 10.1038/ncomms6131; (*b*) M. I. Hashim, H. T. M. Le, T.-H. Chen, Y.-S. Chen, O. Daugulis, C.-W. Hsu, A. J. Jacobson, W. Kaveevivitchai, X. Liang, T. Makarenko, O. Š. Miljanić, I. Popovs, H. V. Tran, X. Wang, C.-H. Wu and J. I. Wu, *J. Am. Chem. Soc.*, 2018, **140**, 6014.

11 (*a*) T.-H. Chen, W. Kaveevivitchai, A. J. Jacobson and O. Š. Miljanić, *Chem. Commun.* 2015, **51**, 14096; (*b*) C. H. Hendon, K. E. Wittering, T.-H. Chen, W. Kaveevivitchai, I. Popov, K. T. Butler, C. C. Wilson, D. L. Cruickshank, O. Š. Miljanić and A. Walsh, *Nano Lett.*, 2015, *15*, 2149; (*c*) Z. Zhang, M. I. Hashim and O. Š. Miljanić, *Chem. Commun.*, 2017, **53**, 10022; (*d*) Z. Zhang, M. I. Hashim, C. Wu, J. I. Wu and O. Š. Miljanić, *Chem. Commun.*, 2018, **54**, 11578.

12 J. Guasch, L. Grisanti, M. Souto, Vega Lloveras, J. Vidal-Gancedo, I. Ratera, A. Painelli, C. Rovira and J. Veciana, *J. Am. Chem. Soc.*, 2013, **135**, 6958.

13 The disordered solvent molecules were removed for clarity.

14 M. J. Turner, J. J. McKinnon, S. K. Wolff, D. J. Grimwood, P. R. Spackman, D. Jayatilaka and M. A. Spackman, CrystalExplorer17 (2017). University of Western Australia. http://hirshfeldsurface.net.

15 Gaussian 16, Revision A.03, M. J. Frisch, G. W. Trucks, H. B. Schlegel, G. E. Scuseria, M. A. Robb, J. R. Cheeseman, G. Scalmani, V. Barone, G. A. Petersson, H. Nakatsuji, X. Li, M. Caricato, A. V. Marenich, J. Bloino, B. G. Janesko, R. Gomperts, B. Mennucci, H. P. Hratchian, J. V. Ortiz, A. F. Izmaylov, J. L. Sonnenberg, D. Williams-Young, F. Ding, F. Lipparini, F. Egidi, J. Goings, B. Peng, A. Petrone, T. Henderson, D. Ranasinghe, V. G. Zakrzewski, J. Gao, N. Rega, G. Zheng, W. Liang, M. Hada, M. Ehara, K. Toyota, R. Fukuda, J. Hasegawa, M. Ishida, T. Nakajima, Y. Honda, O. Kitao, H. Nakai, T. Vreven, K. Throssell, J. A. Montgomery, Jr., J. E. Peralta, F. Ogliaro, M. J. Bearpark, J. J. Heyd, E. N. Brothers, K. N. Kudin, V. N. Staroverov, T. A. Keith, R. Kobayashi, J. Normand, K. Raghavachari, A. P. Rendell, J. C. Burant, S. S. Iyengar, J. Tomasi, M. Cossi, J. M. Millam, M. Klene, C. Adamo, R. Cammi, J. W. Ochterski, R. L. Martin, K. Morokuma, O. Farkas, J. B. Foresman, and D. J. Fox, Gaussian, Inc., Wallingford CT, 2016.

Graphical abstract